Probing strong-field gravity and black holes with gravitational waves

S. A. Hughes[1]

Department of Physics and MIT Kavli Institute, Massachusetts Institute of Technology, 77 Massachusetts Avenue, Cambridge, MA, 02139 United States

Abstract

Gravitational wave observations will be excellent tools for making precise measurements of processes that occur in very strong-field regions of spacetime. Extreme mass ratio systems, formed by the capture of a stellar mass body compact by a massive black hole, will be targets for planned space-based interferometers such as LISA and DECIGO. These systems will be especially powerful tools for testing the spacetime nature of black hole candidates. In this writeup of the talk I gave at JGRG19, I describe how the properties of black holes are imprinted on their waveforms, and how measurements can be used to study these properties and thereby learn about the astrophysics of black holes and about strong-field gravity.

Detectors for measuring gravitational waves (GWs) have recently completed their first multiyear data runs. As this article is written, some of these detectors are being run at "enhanced" sensitivity. It is expected that a final upgrade to "advanced" sensitivity will be needed in order for GWs from astrophysical sources to be measured regularly. Once that state is reached, we can turn this process around, using the GWs that we measure to learn about their sources, using GWs for observational astronomy. The purpose of this article (and the talk on which it is based) is to give a brief review of the state of this field, focusing in particular on how the characteristics of black holes and strong-field gravity are imprinted on a system's GWs.

1 Gravitational waves: Physics and astrophysics

We begin with a brief description of how GWs arise in general realtivity (GR). Our purpose is to introduce the main concepts which describe this phenomenon; later, we will revisit this calculation, showing how to go to higher order in order to describe realistic astrophysical sources. We conclude this section with a quick summary of the astrophysics of binary GW sources.

1.1 Leading waveform

We begin by considering "weak" gravity, so that spacetime is nearly that of special relativity,

$$g_{\alpha\beta} = \eta_{\alpha\beta} + h_{\alpha\beta} \ . \tag{1}$$

Take the correction to flat spacetime to be small, so that we can linearize in $h_{\alpha\beta}$ when we build our curvature tensors. The Einstein tensor in particular becomes

$$G_{\alpha\beta} = \frac{1}{2}\left(\partial_\alpha\partial^\mu h_{\mu\beta} + \partial_\beta\partial^\mu h_{\mu\alpha} - \partial_\alpha\partial_\beta h - \Box h_{\alpha\beta} + \eta_{\alpha\beta}\Box h - \eta_{\alpha\beta}\partial^\mu\partial^\nu h_{\mu\nu}\right) \ , \tag{2}$$

where $h \equiv \eta^{\alpha\beta}h_{\alpha\beta}$ is the trace of $h_{\alpha\beta}$, and $\Box \equiv \eta^{\alpha\beta}\partial_\alpha\partial_\beta$ is the flat spacetime wave operator.

Equation (2) is rather messy. To clean it up, we first introduce the *trace-reversed* metric perturbation $\bar{h}_{\alpha\beta} \equiv h_{\alpha\beta} - (1/2)\eta_{\alpha\beta}h$. With this definition, Eq. (5) becomes

$$G_{\alpha\beta} = \frac{1}{2}\left(\partial_\alpha\partial^\mu \bar{h}_{\mu\beta} + \partial_\beta\partial^\mu \bar{h}_{\mu\alpha} - \Box\bar{h}_{\alpha\beta} - \eta_{\alpha\beta}\partial^\mu\partial^\nu \bar{h}_{\mu\nu}\right) \ . \tag{3}$$

[1]Email address: sahughes@mit.edu

Next, we take advantage of the *gauge-freedom* of linearized gravity. In electrodynamics, we may adjust the potential by the gradient of a scalar, $A_\mu \to A_\mu - \partial_\mu \Lambda$. This leaves the field tensor $F_{\mu\nu} = \partial_\mu A_\nu - \partial_\nu A_\mu$ unchanged. In linearized GR, a similar operation follows by adjusting coordinates: If one changes coordinates $x^\alpha \to x^\alpha + \xi^\alpha$ (requiring $\partial_\mu \xi^\alpha \ll 1$), then

$$h_{\mu\nu} \to h_{\mu\nu} - \partial_\mu \xi_\nu - \partial_\nu \xi_\mu \ . \tag{4}$$

One can easily show that changing gauge leaves all curvature tensors unchanged.

We take advantage of our gauge freedom to choose ξ^α so that $\partial^\mu \bar{h}_{\mu\nu} = 0$. This is called "Lorenz gauge" in analogy with the electrodynamic Lorenz gauge condition $\partial^\mu A_\mu = 0$. This simplifies our Einstein tensor considerably, yielding

$$G_{\alpha\beta} = -\frac{1}{2}\Box \bar{h}_{\alpha\beta} \ . \tag{5}$$

The Einstein equation for linearized gravity thus takes the simple form

$$\Box \bar{h}_{\alpha\beta} = -\frac{16\pi G}{c^4} T_{\alpha\beta} \ . \tag{6}$$

Using a radiative Green's function [e.g., [1], Sec. 12.11], we find the solution

$$\bar{h}_{\alpha\beta}(\mathbf{x}, t) = \frac{4G}{c^4} \int \frac{T_{\alpha\beta}(\mathbf{x}', t - |\mathbf{x} - \mathbf{x}'|/c)}{|\mathbf{x} - \mathbf{x}'|} d^3x' \ . \tag{7}$$

Here, $\mathbf{x}$ is a spatial "field point," where $\bar{h}_{\alpha\beta}$ is evaluated, and $\mathbf{x}'$ is a "source point," the spatial coordinate we integrate over the source's extent. Notice that the solution at t depends on what happens to the source at *retarded time* $t - |\mathbf{x} - \mathbf{x}'|/c$. Information must causally propagate from $\mathbf{x}'$ to $\mathbf{x}$.

Equation (7) is an exact solution to the linearized field equation. It gives the unfortunate impression that every component of the metric perturbation is radiative. Just as one can choose a gauge such that an isolated point charge has an oscillatory potential, the Lorenz gauge makes *all* components of the metric appear radiative, even if they are static[2]. Fortunately, it is not difficult to see that only a subset of the metric represents the radiative degrees of freedom in *all* gauges. We will only quote the result here; interested readers can find the full calculation in Ref. [3], Sec. 2.2: *Given a solution $h_{\alpha\beta}$ to the linearized Einstein field equations, only the* **spatial**, **transverse**, *and* **traceless** *components $h_{ij}^{\rm TT}$ describe the spacetime's gravitational radiation in a gauge-invariant manner.* Traceless means

$$\delta_{ij} h_{ij}^{\rm TT} = 0 \ ; \tag{8}$$

"transverse" means

$$\partial_i h_{ij}^{\rm TT} = 0 \ . \tag{9}$$

Expanding $h_{ij}^{\rm TT}$ in Fourier modes, we see that Eq. (9) requires $h_{ij}^{\rm TT}$ to be orthogonal (in space) to each mode's wave vector $\mathbf{k}$.

Conditions (8) and (9) make it simple to construct $h_{ij}^{\rm TT}$ given some h_{ij}. Let n_i denote components of the unit vector along the propagation direction. The tensor

$$P_{ij} = \delta_{ij} - n_i n_j \tag{10}$$

projects spatial components orthogonal to $\mathbf{n}$. It is then simple to verify that

$$h_{ij}^{\rm TT} = h_{kl} \left(P_{ki} P_{lj} - \frac{1}{2} P_{kl} P_{ij} \right) \tag{11}$$

represents the "TT" metric perturbation. We can now manipulate the solution (7) into

$$h_{ij}^{\rm TT} = \frac{2}{D} \frac{G}{c^4} \frac{d^2 I_{kl}}{dt^2} \left(P_{ik} P_{jl} - \frac{1}{2} P_{kl} P_{ij} \right) \ , \tag{12}$$

[2] In the electromagnetic case, it is unambiguous which *field* components are radiative and which are static. Similarly, one can always tell which *curvature* components are radiative and which are static. Eddington [2] appears to have been the first to use the curvature tensor to categorize gravitational degrees of freedom in this way.

where D is distance to the source, and where

$$I_{ij} = \int x^{i'} x^{j'} T_{tt}(\mathbf{x}', t)\, d^3x' \tag{13}$$

is the source's *quadrupole moment*. It is straightforward to show that the trace $I \equiv I_{ii}$ does not contribute to Eq. (12), so it is common to use the "reduced" quadrupole moment,

$$\mathcal{I}_{ij} = I_{ij} - \frac{1}{3}\delta_{ij} I \; . \tag{14}$$

The waveform then takes the form in which it is usually presented,

$$h_{ij}^{\rm TT} = \frac{2}{R}\frac{G}{c^4}\frac{d^2\mathcal{I}_{kl}}{dt^2}\left(P_{ik}P_{jl} - \frac{1}{2}P_{kl}P_{ij}\right) \; , \tag{15}$$

the *quadrupole formula* for GW emission.

GWs also carry energy from their source. Isaacson [4] first carefully analyzed this in a tensorial manner, showing that GWs produce a stress-energy tensor given by

$$T_{\mu\nu}^{\rm GW} = \frac{c^4}{32\pi G}\langle \hat{\nabla}_\mu h_{\alpha\beta} \hat{\nabla}_\nu h^{\alpha\beta} \rangle \; , \tag{16}$$

where $\hat{\nabla}_\mu$ denotes a covariant derivative in the background spacetime. (This assumes the waveform is in a gauge such that it is transverse and traceless; more general expressions exist.) Notice that the energy content is quadratic in the wave amplitude; computing it correctly requires taking our perturbative analysis to second order. We defer the details of this derivation to Ref. [4].

Now consider a binary system with Newtonian orbital dynamics, radiating GWs according to Eq. (15) and evolving by energy and angular momentum carried off in accordance with Eq. (16). Begin with the binary's members in circular orbit of separation R. This binary has orbital energy

$$E^{\rm orb} = \frac{1}{2}m_1 v_1^2 + \frac{1}{2}m_2 v_2^2 - \frac{G m_1 m_2}{R} = -\frac{G\mu M}{2R} \; , \tag{17}$$

(where $M = m_1 + m_2$ and $\mu = m_1 m_2/M$) and orbital frequency

$$\Omega_{\rm orb} = \sqrt{\frac{GM}{R^3}} \; . \tag{18}$$

Far from the source, Eq. (16) tells us the flux of energy carried by GWs:

$$\frac{dE^{\rm GW}}{dA dt} = \frac{c^4}{32\pi G}\langle \partial_t h_{ij}^{\rm TT} \partial_k h_{ij}^{\rm TT} \rangle n^k \; . \tag{19}$$

Plugging in Eq. (15) and integrating over the sphere, we find

$$\frac{dE}{dt}^{\rm GW} = \int dA \, \frac{dE}{dA dt} = \frac{G}{5c^5}\left\langle \frac{d^3\mathcal{I}_{ij}}{dt^3}\frac{d^3\mathcal{I}_{ij}}{dt^3} \right\rangle \; . \tag{20}$$

For the Newtonian binary,

$$\mathcal{I}_{ij} = \mu\left(x_i x_j - \frac{1}{3}R^2\delta_{ij}\right) \; ; \tag{21}$$

we choose coordinates such that the components of the separation vector are $x_1 = R\cos\Omega_{\rm orb}t$, $x_2 = R\sin\Omega_{\rm orb}t$, $x_3 = 0$. Inserting into Eq. (20), we find

$$\frac{dE}{dt}^{\rm GW} = \frac{32}{5}\frac{G}{c^5}\mu^2 R^4 \Omega^6 \; . \tag{22}$$

We now assert that the binary evolves quasi-statically — any radiation carried off by GWs is accounted for by the evolution of its orbital energy, $dE^{\rm orb}/dt + dE^{\rm GW}/dt = 0$. Allow the orbital radius to slowly change in time, so that $dE^{\rm orb}/dt = (dE^{\rm orb}/dR)(dR/dt)$. Combining this rule with Eq. (22), we find

$$R(t) = \left[\frac{256G^3\mu M^2(t_c - t)}{5c^5}\right]^{1/4} . \tag{23}$$

This in turn tells us that the orbital frequency changes according to

$$\Omega_{\rm orb}(t) = \left[\frac{5c^5}{256(G\mathcal{M})^{5/3}(t_c - t)}\right]^{3/8} . \tag{24}$$

We have introduced the *chirp mass* $\mathcal{M} \equiv \mu^{3/5}M^{2/5}$, so called because it sets the rate at which the binary sweeps upward in frequency, or "chirps." We have also introduced the coalescence time t_c, which formally describes when the separation goes to zero (or when frequency goes to infinity). Corrections for eccentricity can be computed by separately accounting for the evolution of the binary's energy and angular momentum; see Ref. [5], Exercise 16.10 for details.

We conclude this section by writing the gravitational waveform predicted for quadrupole emission from the Newtonian, circular binary. Evaluating Eq. (15), we find that h_{ij} has two polarizations. These are labeled "plus" and "cross," from the lines of force associated with their tidal stretch and squeeze:

$$\begin{aligned} h_+ &= -\frac{2G\mathcal{M}}{c^2 D}\left(\frac{\pi G\mathcal{M}f}{c^3}\right)^{2/3}(1+\cos^2\iota)\cos 2\Phi_N(t) , \\ h_\times &= -\frac{4G\mathcal{M}}{c^2 D}\left(\frac{\pi G\mathcal{M}f}{c^3}\right)^{2/3}\cos\iota\sin 2\Phi_N(t) , \end{aligned} \tag{25}$$

where the phase

$$\Phi_N(t) = \int \Omega_{\rm orb}\, dt = \Phi_c - \left[\frac{c^3(t_c - t)}{5G\mathcal{M}}\right]^{5/8} , \tag{26}$$

and where $f = (1/\pi)d\Phi_N/dt$ is the GW frequency. The system's inclination ι is just the projection of its orbital angular momentum, $\mathbf{L}$, to the wave's direction of propagation $\mathbf{n}$: $\cos\iota = \hat{\mathbf{L}}\cdot\mathbf{n}$ (where $\hat{\mathbf{L}} = \mathbf{L}/|\mathbf{L}|$). Note that h_+ and $h_\times$ depend on, and thus encode, the chirp mass, distance, the position on the sky (via the direction vector $\mathbf{n}$), and the orientation of the binary's orbital plane (via $\hat{\mathbf{L}}$). In later discussion, we will amend Eq. (25) and (26) to include higher order contributions to the binary's waves and evolution.

1.2 Astrophysical binary sources

The binary example considered in the previous section is particularly germane since compact binary systems are among the most important astrophysical sources of GWs. Indeed, our best data on GWs and GW sources comes from observations of *binary pulsar* systems, pairs of neutron stars at least one of which is a pulsar. The pulsar member of the pair acts as an outstanding clock, allowing the properties of the binary to be mapped with great precision.

Some binary neutron stars are in such strong field orbits that the evolution of the binary's orbital period due to GW emission can be discerned over long observational baselines. The prototypical example is the first such system discovered, PSR 1913+16. Over 30 years of study have found extraordinary agreement between prediction and observation for the evolution of this system's orbit [6]. Additional inspiraling systems have been discovered; in all cases for which we have enough data to discern period evolution, the data agree with theory to within measurement precision [7–11]. At least one additional recently discovered system is likely to show a measurable inspiral in the next few years [12].

Turn from binary neutron stars to compact binaries more generally. Such systems are organized most naturally by their masses. At the low end we have *stellar-mass* binaries, including binary pulsars. The data on these binaries are quite solid, since we can tie models for their birth and evolution to observations. At least some fraction of short gamma-ray bursts are likely to be associated with the mergers of neutron

star-neutron star (NS-NS) or black hole-neutron star (BH-NS) systems [13, 14]; as such, gamma-ray telescopes may already be telling us about compact binary merger many times per year [15].

There is also evidence that nature produces *supermassive* binaries, in which the members are black holes with $M \sim 10^6 - 10^8\,M_\odot$ such as are found at the centers of galaxies. Theoretical arguments combining hierarchical galaxy growth scenarios with the hypothesis that most galaxies host black holes generically predict the formation of such binaries. We have now identified many systems with properties indicating that they may host such binaries. The evidence includes active galaxies with double cores [16–18]; systems with doubly-peaked emission lines [19, 20]; helical radio jets [21–23]; and periodic or semi-periodic systems, such as the blazar OJ287 [24]. As surveys go deeper and resolution improves, we may expect the catalog of candidate supermassive black hole binaries to expand.

Now consider theoretical models. Assuming that our galaxy is typical and that the inferred density of NS-NS systems in the Milky Way carries over to similar galaxies (correcting for factors such as typical stellar age and the proportion of stars that form neutron stars), we can estimate the rate at which binary systems merge in the universe. References [25] and [26] first made such estimates, finding a "middle-of-the-road" rate that about 3 binaries per year merge to a distance of 200 Mpc. More recent calculations based on later surveys and observations of NS-NS systems have amended this number somewhat; the total number expected to be measured by advanced detectors is around several tens per year. See, for example, [27] for a detailed discussion of methodology.

Another technique uses population synthesis. These calculations combine data on the observed distribution of stellar binaries with models for how stars evolve. This allows us to estimate the rate of formation and merger for systems which we cannot at present observe, such as stellar mass black hole-black hole (BH-BH) binaries, or for which we have only circumstantial evidence, such as neutron star-black hole (NS-BH) binaries (which presumably form some fraction of short gamma ray bursts). A disadvantage is that the models of stellar evolution in binaries have many uncertainties. There are multiple branch points in binary evolution, such as whether the binary remains bound following each supernova, and whether the binary survives common envelope evolution. As a consequence, the population synthesis predictions can be quite diverse. Though different groups generally agree well with the rates for NS-NS systems (by design), their predictions for NS-BH and BH-BH systems differ by quite a bit. New data are needed to clear the theoretical cobwebs.

Binaries can also form dynamically in dense environments, such as globular clusters. The most massive bodies will tend to sink to a cluster's core through mass segregation [28]; as such, the core will become populated with the heaviest bodies, either stars which will evolve into compact objects, or the compact objects themselves. As those objects interact with one another, they will tend to form massive binaries; calculations show that the production of BH-BH binaries is particularly favored. It is thus likely that globular clusters will act as "engines" for the production of massive compact binaries [29–31].

The hierarchical growth scenario for galaxies, coupled with the hypothesis that most galactic bulges host large black holes, generically predicts the formation of supermassive binaries, especially at high redshifts when mergers were common. The first careful discussion of this was by Begelman, Blandford, and Rees [21]. The coevolution of black holes and galaxies in hierarchical scenarios has now become a very active focus of research (e.g., Refs. [32–34]). Galaxy mergers appear to be a natural mechanism to bring "fuel" to one or both black holes, igniting quasar activity; the formation of a binary may thus be associated with the duty cycle of quasars [35–37]. Such scenarios typically find that most black hole mergers come at fairly high redshift ($z \gtrsim 3$ or so), and that the bulk of a given black hole's mass is due to gas it has accreted over its growth.

A subset of binaries in the supermassive range are of particular interest to the relativity theorist. These binaries form by the capture of a "small" $(1 - 100\,M_\odot)$ compact object onto an orbit around a black hole in a galactic center. Such binaries form dynamically through stellar interactions [38, 39]; the formation rate predicted by most models is typically $\sim 10^{-7}$ extreme mass ratio binaries per galaxy per year [39]. If the inspiraling object is a white dwarf or star, it could tidally disrupt as it comes close to the massive black hole, producing an x-ray or gamma-ray flare [40, 41]. If the inspiraling object is a neutron star or black hole, it will be swallowed whole by the large black hole. As such, it will almost certainly be electromagnetically quiet; however, its GW signature will be loud, and is a particularly interesting target.

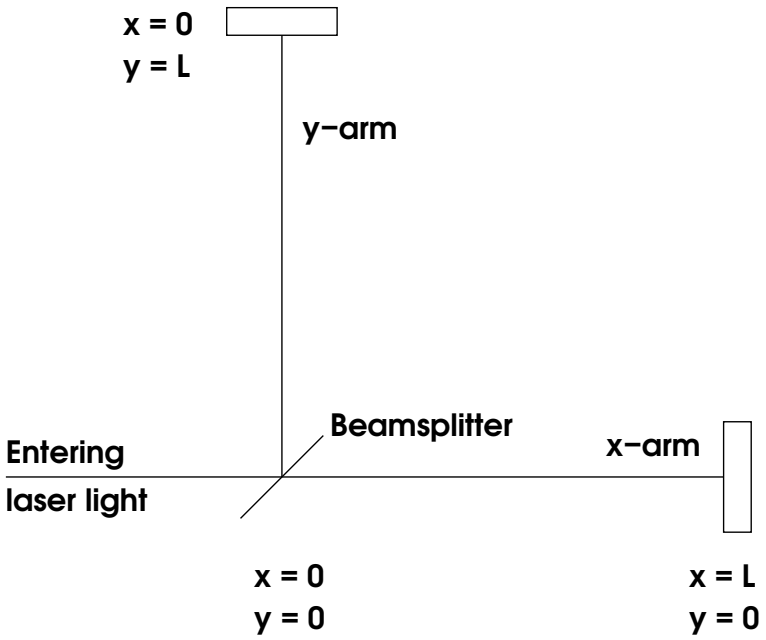

Figure 1: Schematic of an interferometer that could be used to detect GWs. Though real interferometers are vastly more complicated, this interferometer topology contains enough detail to illustrate the principle by which such measurements are made.

2 Measuring gravitational waves: Principles and experiments

Before moving to a discussion of how black hole characteristics and strong-field physics are imprinted on GWs, let us briefly summarize the key principles by which a GW interferometer operators. Begin with the simple limit in which we treat the spacetime in which our detector lives as flat plus a simple GW propagating down our coordinate system's z-axis:

$$ds^2 = -c^2dt^2 + (1+h)dx^2 + (1-h)dy^2 + dz^2 \ , \tag{27}$$

where $h = h(t-z)$. We neglect the influence of the earth (clearly important for terrestrial experiments) and the solar system (which dominates the spacetime of space-based detectors). Corrections describing these influences can be added; we neglect them as they vary on much longer timescales than the GWs.

Figure 1 sketches an interferometer that can measure a GW. Begin by examining the geodesics describing the masses at the ends of the arms, and the beam splitter at the center. Take these objects to be initially at rest, so that $(dx^\mu/d\tau)_{\rm before} \doteq (c,0,0,0)$. The GW shifts this velocity by an amount of order the wave strain: $(dx^\mu/d\tau)_{\rm after} = (dx^\mu/d\tau)_{\rm before} + \mathcal{O}(h)$. Now examine the geodesic equation:

$$\frac{d^2x^j}{d\tau^2} + \Gamma^j{}_{\alpha\beta}\frac{dx^\alpha}{d\tau}\frac{dx^\beta}{d\tau} = 0 \ . \tag{28}$$

All components of the connection are $\mathcal{O}(h)$. Combining this with our argument for how the GW affects the various velocities, we have

$$\frac{d^2x^j}{d\tau^2} + \Gamma^j{}_{00}\frac{dx^0}{d\tau}\frac{dx^0}{d\tau} + \mathcal{O}(h^2) = 0 \ . \tag{29}$$

It is simple to show that the connection coefficient $\Gamma^j{}_{00} = 0$, as the relevant metric components are all constant. We conclude that

$$\frac{d^2x^j}{d\tau^2} = 0 \ . \tag{30}$$

In other words, *the test masses are unaccelerated to leading order in the GW amplitude h.*

This seems to say that the GW has no impact! However, the geodesic equation describes motion *with respect to specified coordinates*. Our coordinates are effectively "comoving" with the interferometer's components. Using the fact that our mirrors are at constant position in these coordinates, it is simple to see that the *proper* length of the arms does change. For instance, the x-arm has a proper length

$$D_x = \int_0^L \sqrt{g_{xx}}\, dx = \int_0^L \sqrt{1+h}\, dx \simeq \int_0^L \left(1+\frac{h}{2}\right) dx = L\left(1+\frac{h}{2}\right) . \tag{31}$$

Likewise, the y-arm has a proper length $D_y = L(1-h/2)$.

This means that the armlengths as measured by a ruler will vary with h. One might worry that, in practice, the ruler will vary with the wave, cancelling the measurement. This does not happen because rulers are not made of freely-falling particles: Its elements are *bound* to one another, and act against the GW. The ruler feels some effect due to the GW, but it is far smaller than the variation in D_x and D_y.

The ruler used by the most sensitive current and planned detectors is based on laser interferometry. We will not describe the details of how a GW is imprinted on the output observable of an interferometer such as that sketch in Fig. 1; for our purposes, it is enough to note that in essence one uses the (highly stable) frequency of the laser as a clock, and times the light travel in the two arms. We recommend the nicely pedagogical article by Faraoni [42] for a clear discussion, as well as a relatively recent analysis by Finn [43] for more detailed discussion.

From basic principles, we now give a brief summary of current and planned detectors. Our goal is not an in-depth discussion, so we refer readers interested in these details to excellent reviews by [44] (which covers in detail the characteristics of the various detectors) and [45] (which covers the interferometry used for space-based detectors). When thinking about GW detectors, a key characteristic is that the frequency of peak sensitivity scales inversely with armlength. The ground-based detectors currently in operation are sensitive to waves oscillating at 10s – 1000s of Hertz. Planned space-based detectors will have sensitivities at much lower frequencies, ranging from 10^{-4} – 0.1 Hz (corresponding to waves with periods of tens of seconds to hours).

The ground-based detectors in operation are LIGO (*Laser Interferometer Gravitational-wave Observatory*), with antennae in Hanford, Washington and Livingston, Louisiana; Virgo near Pisa, Italy; and GEO near Hanover, Germany. The LIGO interferometers have 4-kilometer arms, and a peak sensitivity near 100 Hz. Virgo has 3-kilometer arms, and sensitivity comparable to the LIGO detectors. GEO has 600-meter arms; as such, its peak sensitivity is at higher frequencies than LIGO and Virgo. Using advanced interferometry techniques, it achieves sensitivity competitive with the kilometer-scale instruments. All of these instruments will be upgraded over the course of the next few years, installing more powerful lasers, and reducing the impact of local ground vibrations. The senstivity of LIGO should be improved by roughly a factor of ten, and the bandwidth increased as well. See [46] for detailed discussion.

There are plans to build additional kilometer-scale instruments. The detector AIGO (*Australian International Gravitational Observatory*) is planned as a detector very similar to LIGO and Virgo, but in Western Australia [47]. This location, far from the other major GW observatories, has great potential to improve the ability of the worldwide GW detector network to determine the characteristics of GW events [48]. The Japanese GW community, building on their experience with the 300-meter TAMA interferometer, hopes to build a 3-kilometer *underground* instrument. Dubbed LCGT (*Large-scale Cryogenic Gravitational-wave Telescope*), the underground location takes advantage of the fact that local ground motions tend to decay fairly rapidly as we move away from the earth's surface. They plan to use cryogenic cooling to reduce noise from thermal vibrations.

In space, the major project is LISA (*Laser Interferometer Space Antenna*), a 5-million kilometer interferometer under development as a joint NASA-ESA mission. LISA will consist of three spacecraft placed in orbits so that their relative positions form an equilateral triangle lagging the earth by 20°, inclined to the ecliptic by 60°; see Fig. 2. The spacecraft are free and do not maintain this constellation precisely; however, their armlength variations occur on a timescale far longer than the periods of their target waves. The review by [45] discusses in great detail how one does interferometry on such a baseline with time-changing armlengths. LISA targets waves with periods of hours to several seconds, a rich band for signals involving massive black holes. The LISA *Pathfinder*, a testbed for some of the mission's components, is scheduled for launch in the very near future [49].

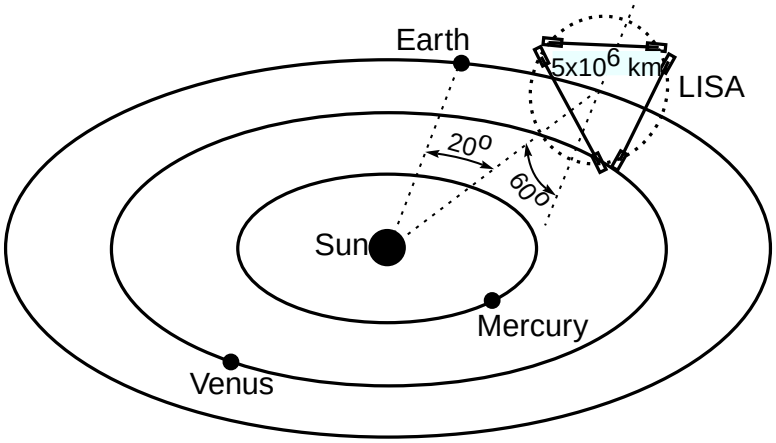

Figure 2: Schematic of the LISA constellation in orbit about the sun. Each arm of the triangle is 5×10^6 km; the centroid of the constellation lags the Earth by 20°, and its plane is inclined to the ecliptic by 60°. Note that the spacecraft orbit freely; there is no formation flying in the LISA configuration. Instead, each spacecraft is in a slightly eccentric, slightly inclined orbit; their individual motions preserve the near-equilateral triangle pattern with high accuracy for a timescale of decades.

Somewhat smaller than LISA, The Japanese GW community has proposed DECIGO (*DECI-hertz Gravitational-wave Observatory*), a space antenna to target a band at roughly 0.1 Hz. This straddles the peak sensitivities of LISA and terrestrial detectors, and may thus act as a bridge for signals that evolve from one band to the other. See Ref. [50] for further discussion.

3 Comparable mass binary waves

We now at last begin to examine how the characteristics of black holes and strong-field gravity are imprinted on the GWs these systems generate. We first must go somewhat beyond the leading-order waveform discussed in Sec. 1.1. After developing the necessary formal tools, we discuss how the interesting characteristics appear in the waves.

3.1 Going beyond leading order

In the analytic treatment of comparable mass binary waves, one begins by considering the *post-Newtonian*, or pN, expansion. This expansion in turn begins by considering the binary in so-called harmonic or deDonder coordinates. In these coordinates, one defines

$$h^{\mu\nu} \equiv \sqrt{-g}g^{\mu\nu} - \eta^{\mu\nu} \ , \tag{32}$$

where g is the determinant of $g_{\mu\nu}$. This looks similar to the flat spacetime perturbation defined in Sec. 1.1; however, we do not assume that h is small. We next impose the gauge condition

$$\partial_\alpha h^{\alpha\beta} = 0 \ . \tag{33}$$

With these definitions, the *exact* Einstein field equations are

$$\Box h^{\alpha\beta} = \frac{16\pi G}{c^4}\tau^{\alpha\beta} \ , \tag{34}$$

where $\Box = \eta^{\alpha\beta}\partial_\alpha\partial_\beta$ is the *flat* spacetime wave operator. The form of Eq. (34) means that the radiative Green's function we used to derive Eq. (7) can be applied here, yielding

$$h^{\alpha\beta} = -\frac{4G}{c^4}\int \frac{\tau_{\alpha\beta}(\mathbf{x}', t - |\mathbf{x} - \mathbf{x}'|/c)}{|\mathbf{x} - \mathbf{x}'|} d^3x' \ . \tag{35}$$

Equation (35) is exact. Note, however, that we never defined the source $\tau^{\alpha\beta}$. It is given by

$$\tau^{\alpha\beta} = (-g)T^{\alpha\beta} + \frac{c^4\Lambda^{\alpha\beta}}{16\pi G} \; ; \tag{36}$$

$T^{\alpha\beta}$ is the usual stress energy tensor, $\Lambda^{\alpha\beta}$ encodes the nonlinear structure of the Einstein field equations:

$$\Lambda^{\alpha\beta} \equiv 16\pi(-g)t_{\rm LL}^{\alpha\beta} + \partial_\nu h^{\alpha\mu}\partial_\mu h^{\beta\nu} - \partial_\mu\partial_\nu h^{\alpha\beta}h^{\mu\nu} \tag{37}$$

$$= N^{\alpha\beta}[h,h] + M^{\alpha\beta}[h,h,h] + L^{\alpha\beta}[h,h,h,h] + \mathcal{O}(h^5) \; . \tag{38}$$

On the first line, $t_{\rm LL}^{\alpha\beta}$ is the Landau-Lifshitz pseudotensor, a quantity which (in certain gauges) allows us to describe how GWs carry energy through spacetime ([51], Sec. 96). On the second line, the term $N^{\alpha\beta}[h,h]$ means a collection of terms quadratic in h and its derivatives, $M^{\alpha\beta}[h,h,h]$ is a cubic term, etc. Our solution $h^{\alpha\beta}$ appears on both the left- and right-hand sides of Eq. (35). Such a structure can be handled very well *iteratively*. We write

$$h^{\alpha\beta} = \sum_{n=1}^{\infty} G^n h_n^{\alpha\beta} \; . \tag{39}$$

The $n = 1$ term is essentially the linearized solution from Sec. 1.1. To go higher, let $\Lambda_n^{\alpha\beta}$ denote the contribution of $\Lambda^{\alpha\beta}$ to the solution $h_n^{\alpha\beta}$. We find

$$\Lambda_2^{\alpha\beta} = N^{\alpha\beta}[h_1,h_1] \; , \tag{40}$$

$$\Lambda_3^{\alpha\beta} = M^{\alpha\beta}[h_1,h_1,h_1] + N^{\alpha\beta}[h_2,h_1] + N^{\alpha\beta}[h_1,h_2] \; , \tag{41}$$

etc.; higher contributions to Λ^{ab} can be found by expanding its definition and gathering terms. By solving the equations which result from this procedure, we can build the spacetime metric and describe the motion of the members of a binary and the radiation that they emit.

We defer details of this construction to the literature (Blanchet's review, Ref. [52], is particularly useful for this purpose), and turn to a study of the interesting features of the pN binary waveform. Take the members of the binary to have masses m_1 and m_2, let their separation be r, and let $\hat{\mathbf{r}}$ point to body 1 from body 2. In the harmonic gauge used for pN theory, the acceleration of body 1 is given by

$$\mathbf{a} = \mathbf{a}_0 + \mathbf{a}_2 + \mathbf{a}_4 + \mathbf{a}_5 + \mathbf{a}_6 + \mathbf{a}_7 \ldots \; . \tag{42}$$

The zeroth term,

$$\mathbf{a}_0 = -\frac{Gm_2}{r^2}\hat{\mathbf{r}}, \tag{43}$$

is the usual Newtonian gravitational acceleration. Each $\mathbf{a}_n$ is a correction of order $(v/c)^n$. The first is

$$\mathbf{a}_2 = \left[\frac{5G^2m_1m_2}{r^3} + \frac{4G^2m_2^2}{r^3} + \frac{Gm_2}{r^2}\left(\frac{3}{2}(\hat{\mathbf{r}}\cdot\mathbf{v_2})^2 - v_1^2 + 4\mathbf{v_1}\cdot\mathbf{v_2} - 2v_2^2\right)\right]\frac{\hat{\mathbf{r}}}{c^2} \; . \tag{44}$$

For the acceleration of body 2 due to body 1, exchange labels 1 and 2 and replace $\hat{\mathbf{r}}$ with $-\hat{\mathbf{r}}$. So far, the pN acceleration has been computed to order $(v/c)^7$. As we go to high order, the expressions for $\mathbf{a}_n$ become quite lengthy. An excellent summary is given in Ref. [52], Eq. (131) and surrounding text.

PN theory also introduces a distinctly non-Newtonian element to binary dynamics: its members' spins *precess* in the binary's curved spacetime. If the spins are $\mathbf{S}_1$ and $\mathbf{S}_2$, one finds [53]

$$\frac{d\mathbf{S}_1}{dt} = \frac{G}{c^2r^3}\left[\left(2+\frac{3}{2}\frac{m_2}{m_1}\right)\mu\sqrt{Mr}\hat{\mathbf{L}}\right]\times\mathbf{S}_1 + \frac{G}{c^2r^3}\left[\frac{1}{2}\mathbf{S}_2 - \frac{3}{2}(\mathbf{S}_2\cdot\hat{\mathbf{L}})\hat{\mathbf{L}}\right]\times\mathbf{S}_1 \; , \tag{45}$$

$$\frac{d\mathbf{S}_2}{dt} = \frac{G}{c^2r^3}\left[\left(2+\frac{3}{2}\frac{m_1}{m_2}\right)\mu\sqrt{Mr}\hat{\mathbf{L}}\right]\times\mathbf{S}_2 + \frac{G}{c^2r^3}\left[\frac{1}{2}\mathbf{S}_1 - \frac{3}{2}(\mathbf{S}_1\cdot\hat{\mathbf{L}})\hat{\mathbf{L}}\right]\times\mathbf{S}_2 \; . \tag{46}$$

We now discuss the ways in which aspects of pN binary dynamics color a system's waves.

3.1.1 Gravitational-wave amplitudes.

Although a binary's *dominant* waves come from variations in its mass quadrupole moment, higher moments also generate GWs. In the pN framework, these moments contribute to the amplitude of a binary's waves beyond the quadrupole form, Eq. (25). Write the gravitational waveform from a source as

$$h_{+,\times} = \frac{2G\mathcal{M}}{c^2 D}\left(\frac{\pi G\mathcal{M}f}{c^3}\right)^{2/3}\left[H^0_{+,\times} + v^{1/2}H^{1/2}_{+,\times} + vH^1_{+,\times} + \ldots\right] , \tag{47}$$

where $v \equiv (\pi GMf/c^3)^{1/3}$ is roughly the orbital speed of the binary's members (normalized to c). The $H^0_{+,\times}$ terms reproduce the waveform presented in Eq. (25). The higher-order terms $H^{1/2}_{+,\times}$ and $H^1_{+,\times}$ can be found in [52], his Eqs. (237) through (241). A key point to note is that these higher-order terms introduce new dependences on the binary's orbital inclination and its masses. As such, measurement of these terms provides additional constraints on the system's characteristics.

3.1.2 Orbital phase.

The motion of a binary's members about each other determines the orbital phase. Specializing to circular orbits, we can determine the orbital frequency from the acceleration of the its members; integrating up this frequency, we define the phase $\Phi(t)$. The first few terms of this phase are given by [54]

$$\begin{aligned}\Phi \;=\; & \Phi_c - \left[\frac{c^3(t_c-t)}{5G\mathcal{M}}\right]^{5/8}\left[1 + \left(\frac{3715}{8064} + \frac{55}{96}\frac{\mu}{M}\right)\Theta^{-1/4} - \frac{3}{16}\left[4\pi - \beta(t)\right]\Theta^{-3/8}\right. \\ & \left. + \left(\frac{9275495}{14450688} + \frac{284875}{258048}\frac{\mu}{M} + \frac{1855}{2048}\frac{\mu^2}{M^2} + \frac{15}{64}\sigma(t)\right)\Theta^{-1/2}\right] ,\end{aligned} \tag{48}$$

where

$$\Theta = \frac{c^3\eta}{5GM}(t_c - t) . \tag{49}$$

The leading term is just the Newtonian quadrupole phase, Eq. (26). Each power of Θ connects to a higher order in the expansion. Equation (48) is taken to "second post-Newtonian" order, meaning that corrections of $(v/c)^4$ are included. Corrections to order $(v/c)^6$ are summarized in [52]. In addition to the chirp mass $\mathcal{M}$, the reduced mass μ enters Φ when higher order terms are included. Including higher pN effects in our wave model makes it possible to determine both chirp mass and reduced mass, fully constraining the binary's masses.

Equation (48) also depends on two parameters, β and σ, which come from the binary's spins and orbit orientation. The "spin-orbit" parameter β is

$$\beta = \frac{1}{2}\sum_{i=1}^{2}\left[113\left(\frac{m_i}{M}\right)^2 + 75\eta\right]\frac{\hat{\mathbf{L}}\cdot\mathbf{S}_i}{m_i^2} ; \tag{50}$$

the "spin-spin" parameter σ is

$$\sigma = \frac{\eta}{48m_1^2m_2^2}\left[721(\hat{\mathbf{L}}\cdot\mathbf{S}_1)(\hat{\mathbf{L}}\cdot\mathbf{S}_2) - 247\mathbf{S}_1\cdot\mathbf{S}_2\right] \tag{51}$$

[54]. These parameters encode valuable information, especially when spin precession is taken into account.

3.1.3 Spin precession.

Although the spin vectors $\mathbf{S}_1$ and $\mathbf{S}_2$ wiggle around according to Eqs. (45) and (46), the system must preserve a notion of *global* angular momentum. Neglecting for a moment the secular evolution of the binary's orbit due to GW emission, pN encodes the notion that the total angular momentum

$$\mathbf{J} = \mathbf{L} + \mathbf{S}_1 + \mathbf{S}_2 \tag{52}$$

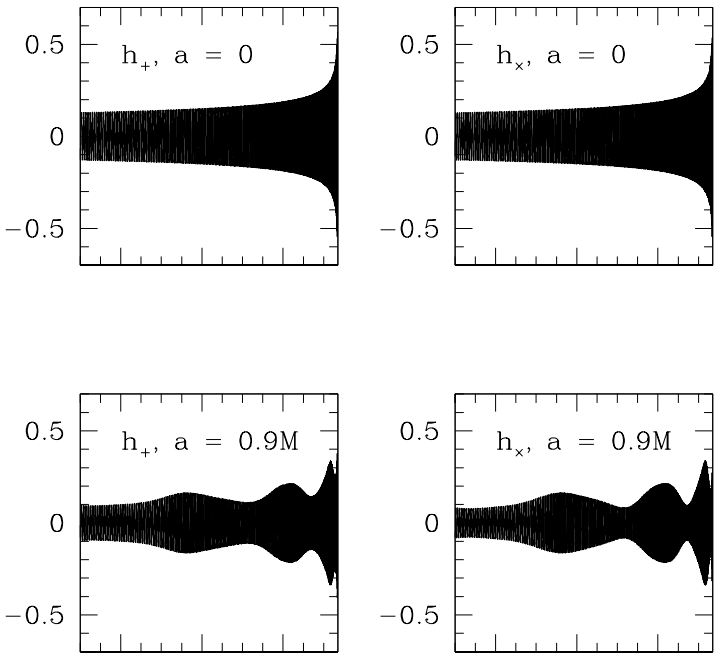

Figure 3: Illustration of precession's impact on a binary's waves. The top panels show h_+ and $h_\times$ for a binary that contains nonspinning black holes; the lower panels show the waveforms for a binary with rapid rapidly rotating ($a = 0.9M$) holes. The strong amplitude modulation is readily apparent in this figure. Less obvious, but also included, is the frequency modulation that enters through the spin-dependent orbital phase parameters β and σ [cf. Eq. (48)].

must be conserved. This means $\mathbf{L}$ must oscillate to compensate for the spins' dynamics, and guarantees that, when spin precession is accounted for in our evolutionary models, the phase parameters β and σ become time varying. Likewise, the inclination angle ι varies with time. Precession thus leads to phase and amplitude modulation of a source's GWs. Figure 3 illustrates precession's impact, showing the late inspiral waves for binaries that are identical aside from spin.

Careful analysis shows that accounting for these effects in our wave model makes it possible to measure the spins of a binary's members, in many cases with excellent precision [55]. By measuring both masses and spins, instruments such as LISA for example become tools for tracking the cosmic evolution of black hole masses and spins, opening a window onto the growth of these objects from early cosmological epochs.

4 Extreme mass ratio binary waves

We conclude by examining waves from extreme mass ratio binaries — stellar mass (roughly $1-100\,M_\odot$) compact bodies spiraling into a much more massive (roughly $10^5-10^7\,M_\odot$) black holes. Such systems are very well modeled using black hole perturbation theory, so we begin with a quick review of this subject.

4.1 Brief overview of black hole perturbation theory

Black hole perturbation theory can be developed much like the weak gravity limit described in Sec. 1.1, replacing the flat spacetime metric $\eta_{\alpha\beta}$ with the spacetime of a black hole:

$$g_{\mu\nu} = g^{\rm BH}_{\mu\nu} + h_{\mu\nu}\ . \tag{53}$$

For astrophysical scenarios, one uses the Schwarzschild (non-rotating black hole) or Kerr (rotating) solutions for $g^{\rm BH}_{\mu\nu}$. It is straightforward (though somewhat tedious) to then develop the Einstein tensor for

this spacetime, keeping terms only to first order in the perturbation h.

This approach works very well when the background is non-rotating,

$$ds^2 = g^{\rm BH}_{\mu\nu} dx^\mu dx^\nu = -\left(1 - \frac{2\hat{M}}{r}\right) dt^2 + \frac{dr^2}{\left(1 - 2\hat{M}/r\right)} + r^2 d\Omega^2 \,, \tag{54}$$

where $d\Omega^2 = d\theta^2 + \sin^2\theta d\phi^2$ and $\hat{M} = GM/c^2$. Our discussion for this special case is adapted from [56]. Because the background is spherically symmetric, we decompose the perturbation into spherical harmonics. For example, under rotations in θ and ϕ, h_{00} should transform as a scalar. We thus put

$$h_{00} = \sum_{lm} a_{lm}(t,r) Y_{lm}(\theta,\phi) \,. \tag{55}$$

The components h_{0i} transform like components of a 3-vector, and can be expanded in vector harmonics; h_{ij} can be expanded in tensor harmonics. One can decompose further with parity: Even harmonics acquire a factor $(-1)^l$ when $(\theta,\phi) \to (\pi-\theta,\phi+\pi)$; odd harmonics acquire a factor $(-1)^{l+1}$.

By imposing these decompositions, choosing a particular gauge, and requiring that the spacetime satisfy the vacuum Einstein equation $G_{\mu\nu} = 0$, we find an equation that governs the perturbations. Somewhat remarkably, the t and r dependence for all components of $h_{\mu\nu}$ for given spherical harmonic indices (l,m) can be constructed from a function $Q(t,r)$ governed by the simple equation

$$\frac{\partial^2 Q}{\partial t^2} - \frac{\partial^2 Q}{\partial r_*^2} - V(r) Q = 0 \,, \tag{56}$$

where $r_* = r + 2\hat{M}\ln(r/2\hat{M} - 1)$. The potential $V(r)$ depends on whether we consider even or odd parity:

$$V_{\rm even}(r) = \left(1 - \frac{2\hat{M}}{r}\right)\left[\frac{2q(q+1)r^3 + 6q^2\hat{M}r^2 + 18q\hat{M}^2 r + 18\hat{M}^3}{r^3\left(qr + 3\hat{M}\right)^2}\right] \,, \tag{57}$$

where $q = (l-1)(l+2)/2$; and

$$V_{\rm odd}(r) = \left(1 - \frac{2\hat{M}}{r}\right)\left[\frac{l(l+1)}{r^2} - \frac{6\hat{M}}{r^3}\right] \,. \tag{58}$$

For even parity, Eq. (56) is the *Zerilli equation* [57]; for odd, it is the *Regge-Wheeler equation* [58]. See [56] for further discussion, including how gauge is chosen and how to construct $h_{\mu\nu}$ from Q. When the spacetime perturbation is due to a body orbiting the black hole, these equations acquire a source term. One can find the waves from an orbiting body by using the source-free equation to build a Green's function, and then integrating over the source.

How does this procedure fare for rotating holes? The background spacetime,

$$ds^2 = -\left(1 - \frac{2\hat{M}r}{\rho^2}\right) dt^2 - \frac{4a\hat{M}r\sin^2\theta}{\rho^2} dt d\phi + \frac{\rho^2}{\Delta} dr^2 + \rho^2 d\theta^2 + \left(r^2 + a^2 + \frac{2\hat{M}ra^2\sin^2\theta}{\rho^2}\right) d\phi^2 \,, \tag{59}$$

where

$$a = \frac{|\vec{S}|}{cM} \,, \qquad \rho^2 = r^2 + a^2\cos^2\theta \,, \qquad \Delta = r^2 - 2\hat{M}r + a^2 \,, \tag{60}$$

is now nonspherical, and the decomposition into spherical harmonics is not useful. One could in principle simply expand $G_{\mu\nu} = 0$ to first order in $h_{\mu\nu}$ and obtain a partial differential equation in t, r, and θ. (The metric is axially symmetric, so we can easily separate the ϕ dependence.)

Rather than expanding the metric, Teukolsky [59] examined perturbations of curvature:

$$R_{\alpha\mu\beta\nu} = R^{\rm BH}_{\alpha\mu\beta\nu} + \delta R_{\alpha\mu\beta\nu} \,. \tag{61}$$

The curvature tensor is invariant to first-order gauge transformations, an attractive feature. This tensor obeys a nonlinear wave equation which can be derived from the Bianchi identity; see [60] for discussion. By expanding this wave equation to linear order in $\delta R_{\alpha\mu\beta\nu}$, Teukolsky showed that perturbations to Kerr black holes are governed by the equation

$$\left[\frac{(r^2+a^2)^2}{\Delta}-a^2\sin^2\theta\right]\partial_t^2\Psi-4\left[r+ia\cos\theta-\frac{\hat{M}(r^2-a^2)}{\Delta}\right]\partial_t\Psi+\frac{4i\hat{M}amr}{\Delta}\partial_t\Psi-\Delta^2\partial_r\left(\Delta^{-1}\partial_r\Psi\right)$$
$$-\frac{1}{\sin\theta}\partial_\theta\left(\sin\theta\partial_\theta\Psi\right)-\left[\frac{a^2}{\Delta}-\frac{1}{\sin^2\theta}\right]m^2\Psi+4im\left[\frac{a(r-\hat{M})}{\Delta}+\frac{i\cos\theta}{\sin^2\theta}\right]\Psi-\left(4\cot^2\theta+2\right)\Psi=\mathcal{T}\,. \tag{62}$$

The field Ψ is a complex quantity built from a combination of components of $\delta R_{\alpha\mu\beta\nu}$. It describes a spacetime's radiation; see [59] for details. (We have assumed $\Psi\propto e^{im\phi}$.) Likewise, $\mathcal{T}$ describes a source function built from the stress-energy tensor describing a small body orbiting the black hole.

Somewhat amazingly, Eq. (62) separates: putting

$$\Psi=\int d\omega\sum_{lm}R_{lm\omega}(r)S_{lm\omega}(\theta)e^{im\phi-i\omega t} \tag{63}$$

and applying a similar decomposition to the source $\mathcal{T}$, we find that $S_{lm\omega}(\theta)$ is a "spin-weighted spheroidal harmonic" (a basis for tensor functions in a non-spherical background), and that $R_{lm\omega}(r)$ is governed by a simple ordinary differential equation. Ψ characterizes Kerr perturbations in much the same way that Q [cf. Eq. (56)] characterizes them for Schwarzschild. Although the perturbation equations are often solved numerically, analytic solutions are known [61], and can dramatically improve one's scheme for solving for black hole perturbations; see Refs. [62, 63].

How do we describe the motion of a small body about a black hole? The most rigorous approach is to enforce $\nabla^\mu T_{\mu\nu}=0$, where $T_{\mu\nu}$ describes the small body in the spacetime of the large black hole. Neglecting the small body's perturbation to the spacetime, we find the geodesic equation $u^\mu\nabla_\mu u^\nu=0$, where u^μ is the small body's 4-velocity. Geodesic black hole orbits have been studied extensively; see, for example, Ref. [64], Chapter 33. They are characterized (up to initial conditions) by three conserved constants: energy E, axial angular momentum L_z, and "Carter's constant" Q. If the black hole does not rotate, Carter's constant is related to the orbit's total angular momentum: $Q(a=0)=\mathbf{L}\cdot\mathbf{L}-L_z^2$. When the black hole rotates rapidly, Q is not so easy to interpret; the idea that it is essentially the rest of the orbit's angular momentum can be useful.

Taking into account perturbations from the small body, $\nabla^\mu T_{\mu\nu}=0$ now implies that the small body follows a "forced" geodesic,

$$u^\mu\hat{\nabla}_\mu u^\nu=f^\nu\,, \tag{64}$$

where $\hat{\nabla}_\mu$ is the covariant derivative in the background spacetime. The novel feature of Eq. (64) is the *self force* f^ν, a correction to the motion of order the small body's spacetime perturbation. The self force is so named because it arises from the body's interaction with its own spacetime correction.

Computing the gravitational self force near a black hole is an active area of current research. It is useful to break the self force into a *dissipative* piece, $f^\nu_{\rm diss}$, which is asymmetric under time reversal, and a *conservative* piece, $f^\nu_{\rm cons}$, which is symmetric. Dissipation causes the "conserved" quantities (E,L_z,Q) to decay, driving inspiral of the small body. Quinn and Wald [65] have shown that the rate at which E and L_z change due to $f^\nu_{\rm diss}$ is identical to what is found when one computes the fluxes of energy and angular momentum encoded by the Isaacson tensor (16).

The conservative self force does not cause orbit decay. "Conserved" constants remain conserved, but the orbits are shifted from the background geodesics. This reflects the fact that, even neglecting dissipation, the small body's motion is determined by the full spacetime, not just the background black hole. Conservative effects shift the orbital frequencies by an amount

$$\delta\Omega_x\sim\Omega_x\times(\mu/M) \tag{65}$$

[where $x \in (\phi, \theta, r)$]. Because the GWs have spectral support at harmonics of the orbital frequencies, these small but non-negligible frequency shifts are directly encoded in the waves that the binary generates. Good discussion and a toy model can be found in [66].

There has been enormous progress in understanding self forces on orbits around non-rotating holes. Barack and Sago [67] have completed an analysis of the full self force for circular orbits about a Schwarzschild black hole; generalization to eccentric orbits is in progress (L. Barack, private communication). An independent approach developed by Detweiler [68] has been found to agree with Barack and Sago extremely well; see [69] for detailed discussion of this comparison.

4.2 Gravitational waves from extreme mass ratio binaries

We now discuss the properties of GWs and GW sources as calculated using perturbation theory. Our goal is to highlight features of the Kerr inspiral waveform. We will neglect the conservative self force, which is not yet understood for the Kerr case well enough to be applied to these waves. When conservative effects are neglected, the binary can be regarded as evolving through a sequence of geodesics, with the sequence determined by the rates at which GWs change the "constants" E, L_z, and Q. Modeling compact binaries in this limit takes three ingredients: First, a description of black hole orbits; second, an algorithm to compute GWs from the orbits, and to infer how the waves' backreaction evolves us from orbit to orbit; and third, a method to integrate along the orbital sequence to build the full waveform. A description of this method is given in [70]; we summarize the main results of these three ingredients here.

4.2.1 Black hole orbits.

Motion near a black hole can be conveniently written in the coordinates of Eq. (59) as $r(t)$, $\theta(t)$, and $\phi(t)$. Because t corresponds to time far from the black hole, this gives a useful description of the motion as measured by distant observers. *Bound* orbits are confined to a region near the hole. They have $r_{\rm min} \le r(t) \le r_{\rm max}$ and $\theta_{\rm min} \le \theta(t) \le \pi - \theta_{\rm min}$, and thus occupy a torus in the 3-space near the hole's event horizon; an example is shown in Fig. 4, taken from [71]. Selecting the constants E, L_z, and Q fully determines $r_{\rm min/max}$ and $\theta_{\rm min}$. It is useful for some discussions to reparameterize the radial motion, defining an eccentricity e and a semi-latus rectum p via

$$r_{\rm min} = \frac{p}{1+e} , \qquad r_{\rm max} = \frac{p}{1-e} . \tag{66}$$

For many bound black hole orbits, $r(t)$, $\theta(t)$, and $\phi(t)$ are periodic [72, 73]. (Exceptions are orbits which plunge into the hole; we discuss these below.) Near the hole, the time to cover the full range of r becomes distinct from the time to cover the θ range, which becomes distinct from the time to cover 2π radians of azimuth. One can say that spacetime curvature splits the Keplerian orbital frequency Ω into Ω_r, Ω_θ, and Ω_ϕ. Figure 5 shows these three frequencies, plotted as functions of semi-major axis A for fixed values of e and $\theta_{\rm min}$. Notice that all three approach $\Omega \propto A^{-3/2}$ for large A.

4.2.2 Gravitational radiation from orbits.

Because their orbits are periodic, GWs from a body orbiting a black hole will have support at harmonics of the orbital frequencies. One can write the two polarizations

$$h_+ + i h_\times = \sum H_{mkn} e^{i\omega_{mkn} t} , \qquad \text{where} \tag{67}$$

$$\omega_{mkn} = m\Omega_\phi + k\Omega_\theta + n\Omega_r . \tag{68}$$

The amplitude H_{mkn} can be found by solving the Teukolsky equation (62) using the decomposition (63); details for the general case can be found in [71].

The expansion (67) does not work well for orbits that plunge into the black hole; those orbits are not periodic, and cannot be expanded using a set of real frequencies. A better way to calculate those waves is to solve the Teukolsky equation (62) *without* introducing the decomposion (63). Results for waves from

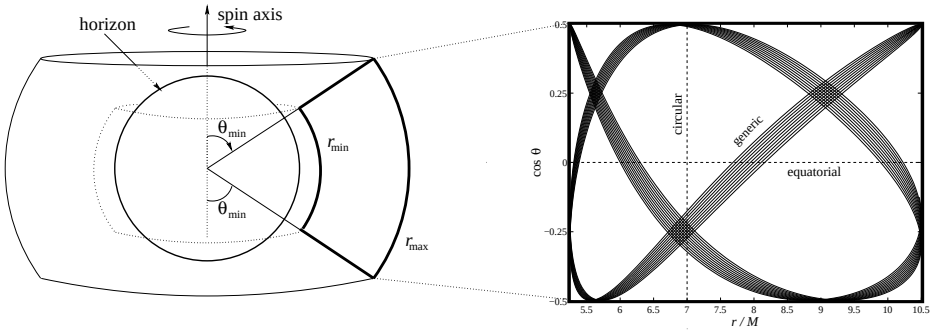

Figure 4: The geometry of a generic Kerr black hole orbit [taken from [71]]. This orbit is about a black hole with spin parameter $a = 0.998M$ (recall $a \leq M$, so this represents a nearly maximally spinning black hole). The range of its radial motion is determined by $p = 7GM/c^2$ (G and c are set to 1 in the figure) and $e = 1/3$; θ ranges from 60° to 120°. The left panel shows the torus in coordinate space this torus occupies. The right panel illustrates how a generic orbit ergodically fills this torus.

plunging orbits in the language of perturbation theory were first given by Damour, Nagar, and Tartaglia [74]; Sundararajan [75] has recently extended the cases that we can model to full generality.

As mentioned above, it is fairly simple to compute the flux of energy $\dot{E}$ and angular momentum $\dot{L}_z$ from the Isaacson tensor, Eq. (16), once the waves are known. Recent work [76] has shown that a similar result describes $\dot{Q}$. Once $\dot{E}$, $\dot{L}_z$, and $\dot{Q}$ are known, it is straightforward to evolve the orbital elements $r_{\rm min/max}$ and $\theta_{\rm min}$, specifying the sequence of orbits through which GWs drive the system. Once that sequence is known, it is straightforward to build the worldline that a small body follows as it spirals into the black hole. From the worldline, we can build a source function $\mathcal{T}(t)$ for Eq. (62) and compute the evolving inspiral waves.

4.3 Mapping black hole spacetimes

Extreme mass ratio GW events may allow a unique and powerful measurement: We may use them to "map" the spacetimes of black holes and test how well they satisfy the stringent requirements of GR. As discussed above, an extreme mass ratio inspiral is essentially a sequence of orbits. Thanks to the mass ratio, the small body moves through this sequence slowly, spending a lot of time "close to" any orbit in the sequence. Also thanks to the mass ratio, each orbit's properties are mostly determined by the larger body. In analogy to *geodesy*, the mapping of earth's gravity with satellite orbits, one can imagine *bothrodesy*[3], the mapping of a black hole's gravity by studying the orbits of inspiraling "satellites."

In more detail, consider first Newtonian gravity. The exterior potential of a body of radius R can be expanded in a set of multipole moments:

$$\Phi_N = -\frac{GM}{r} + G\sum_{l=2}^{\infty}\left(\frac{R}{r}\right)^{l+1} M_{lm}Y_{lm}(\theta,\phi)\ . \tag{69}$$

Studying orbits allows us to map the potential Φ_N, and thus to infer the moments M_{lm}. By enforcing Poisson's equation in the interior, $\nabla^2\Phi_N = 4\pi G\rho$, and then matching at the surface R, one can relate the moments M_{lm} to the distribution of matter. In this way, orbits allow us to map in detail the distribution of matter in a body like the earth.

Bothrodesy applies the same idea to a black hole. The spacetime of any stationary, axisymmetric body can be described by a set of "mass moments" M_l, similar to the M_{lm} of Eq. (69); and a set of "current moments" S_l which describe the distribution of mass-energy's *flow*. The moments of a black hole take a simple, special form: for a Kerr black hole (59) with mass M and spin parameter a,

$$M_l + iS_l = M(ia)^l\ . \tag{70}$$

[3]This name was coined by Sterl Phinney, and comes from the word $\beta o\theta\rho o\varsigma$, which refers to a sacrificial pit in ancient Greek. This author offers an apology to speakers of modern Greek.

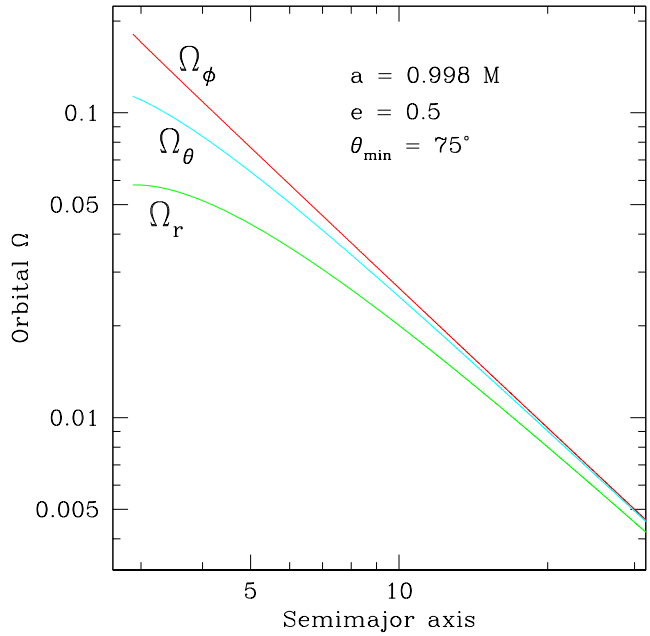

Figure 5: Orbital frequencies for generic Kerr black hole orbits. We vary the orbits' semilatus rectum p, but fix eccentricity $e = 0.5$ and inclination parameter $\theta_{\rm min} = 75°$. Our results are plotted as a function of semimajor axis $A = p/\sqrt{1-e^2}$. All three frequencies asymptote to the Keplerian value $\Omega = \sqrt{GM/A^3}$ in the weak field, but differ significantly from each other in the strong field.

A black hole has a mass moment $M_0 = M$ and a current moment $S_1 = aM$ (i.e., the magnitude of its spin is aM, modulo factors of G and c). *Once those moments are known, all other moments are fixed if the Kerr solution describes the spacetime.* This is a restatement of the "no hair" theorem [77, 78] that a black hole's properties are set by its mass and spin.

The facts that an object's spacetime and orbits are determined by its multipoles, and that the Kerr moments take such a simple form, suggests a consistency test: Develop an algorithm for mapping the multipolar structure by studying orbits, and check that the $l \geq 2$ moments satisfy Eq. (70). Ryan [79] first demonstrated that such a measurement can be done, and Brink [80] has recently clarified what must be done for such measurements to be done in practice. Collins and Hughes [81] took the first steps in formulating this question as a null experiment (with the Schwarzschild solution as the null hypothesis). Glampedakis and Babak [82] formulated a similar approach appropriate to Kerr black holes; Vigeland and Hughes [83] have recently extended the Collins and Hughes formalism in that direction.

A robust test of the Kerr solution is thus a very likely outcome of measuring waves from extreme mass ratio captures. If testing metrics is not your cup of tea, precision black hole metrology may be: In the process of mapping a spacetime, one measures with exquisite accuracy both the mass and the spin of the large black hole. Barack and Cutler [84] have found that in most cases these events will allow us to determine both the mass and the spin of the large black hole with 0.1% errors are better. GW measurements will give us a precise picture of these amazing objects.

Acknowledgments

Portions of this proceedings article were adapted from previous reviews I have written or cowritten (Refs. [3, 60]). Much of the research discussed here was done in collaboration with my collaborators Steve Drasco, Éanna Flanagan, and Gaurav Khanna, as well as my current and former graduate students Nathan Collins, Ryan Lang, Pranesh Sundararajan, and Sarah Vigeland. My group's research in gravitational waves and

compact binaries is supported by NSF Grant PHY-0449884 and NASA Grant NNX08AL42G; some of the work discussed here was also supported by NASA Grant NNG05G105G and the MIT Class of 1956 Career Development Fund. I gratefully acknowledge the support of the Adam J. Burgasser Chair in Astrophysics at MIT in completing this conference writeup.

References

[1] J. D. Jackson, *Classical electrodynamics* (Wiley, New York, 1975).

[2] A. S. Eddington, Proc. Roy. Soc. Lond. **A102**, 268 (1922).

[3] E. E. Flanagan and S. A. Hughes, New J. Phys. **7**, 204 (2005).

[4] R. A. Isaacson, Phys. Rev. **166**, 1272 (1968).

[5] S. L. Shapiro and S. A. Teukolsky, *Black Holes, White Dwarfs, and Neutron Stars: The Physics of Compact Objects* (Wiley, New York, 1983).

[6] J. M. Weisberg and J. H. Taylor, in *The Relativistic Binary Pulsa B1913+16: Thirty Years of Observations and Analysis*, Astron. Soc. of the Pac. Conf. Ser. **328**, 25 (2005).

[7] I. H. Stairs et al., Astrophys. J. **505**, 352 (1998).

[8] D. J. Nice et al., Astrophys. J. **634**, 1242 (2005).

[9] B. A. Jacoby et al., Astrophys. J. Lett. **644**, L113 (2006).

[10] M. Kramer and I. H. Stairs, Ann. Rev. Astron. Astrophys. **46**, 541 (2008).

[11] N. D. R. Bhat, M. Bailes, and J. P. W. Verbiest, Phys. Rev. D **77**, 124017 (2008).

[12] L. Kasian, AIP Conf. Ser. **983**, 485 (2008).

[13] D. Eichler, M. Livio, T. Piran, and D. N. Schramm, Nature **340**, 126 (1989).

[14] D. B. Fox et al., Nature **437**, 845 (2005).

[15] E. Nakar, A. Gal-Yam, and D. B. Fox, Astrophys. J. **650**, 281 (2006).

[16] S. Komossa et al., Astrophys. J. Lett. **582**, L15 (2003).

[17] H. L. Maness et al., Astrophys. J. **602**, 123 (2004).

[18] C. Rodriguez et al., Astrophys. J. **646**, 49 (2006).

[19] H. Zhou, T. Wang, X. Zhang, X. Dong, and C. Li, Astrophys. J. Lett. **604**, L33 (2004).

[20] B. F. Gerke, Astrophys. J. Lett. **660**, L23 (2007).

[21] M. C. Begelman, R. D. Blandford, and M. J. Rees, Nature **287**, 307 (1980).

[22] J. E. Conway and J. M. Wrobel, Astrophys. J. **439**, 98 (1995).

[23] A. P. Lobanov and J. Roland, Astron. Astrophys. **431**, 831 (2005).

[24] M. J. Valtonen et al., Nature **452**, 851 (2008).

[25] R. Narayan, T. Piran, and A. Shemi, Astrophys. J. Lett. **379**, L17 (1991).

[26] E. S. Phinney, Astrophys. J. Lett. **380**, L17 (1991).

[27] V. Kalogera, K. Belczynski, C. Kim, R. O'Shaughnessy, and B. Willems, Phys. Rep. **442**, 75 (2007).

[28] L. J. Spitzer, Astrophys. J. Lett. **148**, 139 (1969).

[29] S. F. Portegies Zwart and S. L. W. McMillan, Astrophys. J. Lett. **528**, L17 (2000).

[30] R. M. O'Leary, R. O'Shaughnessy, and F. A. Rasio, Phys. Rev. D **76**, 6 (2007).

[31] A. D. Mackey, M. I. Wilkinson, M. B. Davies, and G. F. Gilmore, Mon. Not. R. Astron. Soc. **386**, 65 (2008).

[32] K. Menou, Z. Haiman, and V. K. Narayanan, Astrophys. J. **558**, 535 (2001).

[33] Q. Yu and S. Tremaine, Mon. Not. R. Astron. Soc. **335**, 965 (2002).

[34] M. Volonteri, F. Haardt, and P. Madau, Astrophys. J. **582**, 559 (2003).

[35] Z. Haiman, L. Ciotti, and J. P. Ostriker, Astrophys. J. **606**, 763 (2004).

[36] P. F. Hopkins, T. J. Cox, D. Kereš, and L. Hernquist, Astrophys. J. Suppl. **175**, 390 (2008).

[37] T. Di Matteo, J. Colberg, V. Springel, L. Hernquist, and D. Sijacki, Astrophys. J. **676**, 33 (2008).

[38] S. Sigurdsson and M. J. Rees, Mon. Not. R. Astron. Soc. **284**, 318 (1997).

[39] C. Hopman and T. Alexander, Astrophys. J. **629**, 362 (2005).

[40] Y. Rathore, R. D. Blandford, and A. E. Broderick, Mon. Not. R. Astron. Soc. **357**, 834 (2005).

[41] K. Menou, Z. Haiman, and K. Menou, New Astron. Rev. **51**, 884 (2008).

[42] V. Faraoni, Gen. Rel. Grav. **39**, 677 (2007).

[43] L. S. Finn, Phys. Rev. D **79**, 022002 (2008).

[44] J. Hough and S. Rowan, Liv. Rev. Rel. **3**, 3 (2000).

[45] M. Tinto and S. V. Dhurandar, Liv. Rev. Rel. **8**, 4 (2005).

[46] P. Fritschel, *Second generation instruments for the Laser Interferometer Gravitational Wave Observatory (LIGO)*, SPIE Conf. Ser. **4856**, 282 (2003).

[47] D. E. McClelland, *Status of the Australian consortium for interferometric gravitational astronomy*, in Proceedings of the 9th Marcel Grossman Meeting, eds. V. G. Gurzadyan, R. T. Jantzen, and R. Ruffini, p. 1864 (2002).

[48] A. C. Searle, S. M. Scott, D. E. McClelland, and L. S. Finn, Phys. Rev. D **73**, 124014 (2006).

[49] S. Vitale, gr-qc/0504062.

[50] S. Kawamura et al., Class. Quantum Grav. **23**, 125 (2006).

[51] L. D. Landau and E. M. Lifschitz, *The classical theory of fields* (Pergamon, London, 1975).

[52] L. Blanchet, Liv. Rev. Rel. **9**, 4 (2006).

[53] K. S. Thorne and J. B. Hartle, Phys. Rev. D **31**, 1815 (1985).

[54] L. Blanchet, T. Damour, B. R. Iyer, C. M. Will, and A. G. Wiseman, Phys. Rev. Lett. **74**, 3515 (1995).

[55] R. N. Lang and S. A. Hughes, Phys. Rev. D **74**, 122001 (2006).

[56] L. Rezzolla, *Gravitational waves from perturbed black holes and relativistic stars*, in ICTP Lecture Series **3** (2003).

[57] F. J. Zerilli, Phys. Rev. D **2**, 2141 (1970).

[58] T. Regge and J. A. Wheeler, Phys. Rev. **108**, 1063 (1957).

[59] S. A. Teukolsky, Astrophys. J. **185**, 635 (1973).

[60] S. A. Hughes, Ann. Rev. Astron. Astrophys. **47**, 107 (2009).

[61] S. Mano, H. Suzuki, and E. Takasugi, Prog. Theo. Phys. **95**, 1079 (1996).

[62] R. Fujita and H. Tagoshi, Prog. Theor. Phys. **112**, 415 (2004).

[63] R. Fujita and H. Tagoshi, Prog. Theor. Phys. **113**, 1165 (2005).

[64] C. W. Misner, K. S. Thorne, and J. A. Wheeler, *Gravitation* (W. H. Freeman and Co., San Francisco, 1973).

[65] T. C. Quinn and R. M. Wald, Phys. Rev. D **60**, 064009 (1999).

[66] A. Pound, E. Poisson, and B. G. Nickel, Phys. Rev. D **72**, 124001 (2005).

[67] L. Barack and N. Sago, Phys. Rev. D **75**, 064021 (2007).

[68] S. Detweiler, Phys. Rev. D **77**, 124026 (2008).

[69] N. Sago, L. Barack, and S. Detweiler, Phys. Rev. D **78**, 124024 (2008).

[70] S. A. Hughes, S. Drasco, E. E. Flanagan, and J. Franklin, Phys. Rev. Lett. **94**, 221101 (2005).

[71] S. Drasco and S. A. Hughes, Phys. Rev. D **73**, 024027 (2006).

[72] W. Schmidt, Class. Quantum Grav. **19**, 2743 (2002).

[73] S. Drasco and S. A. Hughes, Phys. Rev. D **69**, 044015 (2004).

[74] A. Nagar, T. Damour, and A. Tartaglia, Class. Quantum Grav. **24**, 109 (2007).

[75] P. A. Sundararajan, Phys. Rev. D **77**, 124050 (2008).

[76] K. Ganz, W. Hikida, H. Nakano, and T. Tanaka, Prog. Theor. Phys. **117**, 1041 (2007).

[77] B. Carter, Phys. Rev. Lett. **26**, 331 (1971).

[78] D. C. Robinson, Phys. Rev. Lett. **34**, 905 (1975).

[79] F. D. Ryan, Phys. Rev. D **52**, 5707 (1995).

[80] J. Brink, Phys. Rev. D **78**, 102001 (2008).

[81] N. A. Collins and S. A. Hughes, Phys. Rev. D **69**, 124022 (2004).

[82] K. Glampedakis and S. Babak, Class. Quantum Grav. **23**, 4167 (2006).

[83] S. J. Vigeland and S. A. Hughes, Phys. Rev. D **81**, 024030 (2010).

[84] L. Barack and C. Cutler, Phys. Rev. D **69**, 082005 (2004).